OPEN ACCESS
CellPress

Cell Reports
Report

Structure of the VipA/B Type VI Secretion Complex Suggests a Contraction-State-Specific Recycling Mechanism

Sebastian Kube,[1] Nicole Kapitein,[2,3] Tomasz Zimniak,[1] Franz Herzog,[1] Axel Mogk,[2,3] and Petra Wendler[1,*]
[1]Gene Center Munich, Ludwig-Maximilians-Universität (LMU) München, Feodor-Lynen-Strasse 25, 81377 Munich, Germany
[2]Zentrum für Molekulare Biologie, University Heidelberg (ZMBH), DKFZ-ZMBH Alliance, Im Neuenheimer Feld 282, 69120 Heidelberg, Germany
[3]Deutsches Krebsforschungszentrum (DKFZ), Im Neuenheimer Feld 282, 69120 Heidelberg, Germany
*Correspondence: wendler@genzentrum.lmu.de
http://dx.doi.org/10.1016/j.celrep.2014.05.034

SUMMARY

The bacterial type VI secretion system is a multicomponent molecular machine directed against eukaryotic host cells and competing bacteria. An intracellular contractile tubular structure that bears functional homology with bacteriophage tails is pivotal for ejection of pathogenic effectors. Here, we present the 6 Å cryoelectron microscopy structure of the contracted *Vibrio cholerae* tubule consisting of the proteins VipA and VipB. We localized VipA and VipB in the protomer and identified structural homology between the C-terminal segment of VipB and the tail-sheath protein of T4 phages. We propose that homologous segments in VipB and T4 phages mediate tubule contraction. We show that in type VI secretion, contraction leads to exposure of the ClpV recognition motif, which is embedded in the type VI-specific four-helix-bundle N-domain of VipB. Disaggregation of the tubules by the AAA+ protein ClpV and recycling of the VipA/B subunits are thereby limited to the contracted state.

INTRODUCTION

Bacteria have evolved a variety of contact-dependent secretion systems to interact with other organisms in their environment (Hayes et al., 2010). The type VI secretion system (T6SS), which is present in a quarter of all proteobacterial genomes, plays a crucial role in bacterial pathogenicity and possibly symbiosis, targeting either eukaryotic or competitor bacterial cells (Coulthurst, 2013; Records, 2011). The overall mechanism and structure of the T6SS is believed to resemble an inverted phage tail puncturing neighboring cells from inside the bacteria (Leiman et al., 2009).

The T6SS core secretion apparatus consists of 13 essential and conserved proteins, some of which display structural homology to bacteriophage components (Cascales and Cambillau, 2012). VgrG (valine-glycine-repeat protein), which forms the tip of the cell-puncturing device together with the PAAR-domain-containing protein VCA0105 (Shneider et al., 2013), is a structural homolog of T4 bacteriophage spike proteins gp27 and gp5 (Leiman et al., 2009; Pukatzki et al., 2007). The secreted homohexameric Hcp (hemolysin coregulated protein) bears similarity to the T4 tail tube protein gp19 (Leiman et al., 2009; Mougous et al., 2006) and also has a chaperone function for secreted effectors (Lossi et al., 2011; Silverman et al., 2013). In addition, the small protein TssE is homologous to the phage baseplate wedge protein gp25 (Leiman et al., 2009; Lossi et al., 2011).

Pivotal to the T6SS are the tubule-forming proteins VipA and VipB (TssB and TssC), which are proposed to trigger pathogen secretion by rapid contraction (Basler et al., 2012). Despite functional similarity between contractile bacteriophage tails and T6SS tubules, VipA (18.5 kDa) and VipB (55.6 kDa) share no significant sequence homology with T4 tail sheath protein gp18. Only weak homologies were found between the C-terminal regions of VipB and gp18 (Leiman and Shneider, 2012). On basis of the functional similarity, it was hypothesized that the VipA/B complex provides the energy to eject the tube-protein-like Hcp structure upon contraction, thereby possibly puncturing the target cell and injecting pathogenic effectors into its interior. The contracted tubule is then disassembled by the AAA+ ATPase ClpV, which recycles VipA/B for reloading of the complex (Basler et al., 2012; Bönemann et al., 2009; Kapitein et al., 2013). Due to the lack of high-resolution structures of the T6SS machinery, the molecular mechanisms of effector ejection and tubule recycling are not very well understood.

Here, we report the cryoelectron microscopy (cryo-EM) reconstruction of the VipA/B tubule in its contracted state at 6 Å resolution. In a hybrid approach of electron microscopic and bioinformatic methods validated by crosslinking mass spectrometry, we were able to localize secondary structure elements of VipA and VipB in the density. We demonstrate that VipB shares structural homology to viral tail-sheath proteins, but also harbors unique elements linked to T6SS-specific functions. Utilizing this structural and functional homology, we deduced a model of the elongated state of the complex and suggest a mechanism for contraction-state-specific T6S recycling.

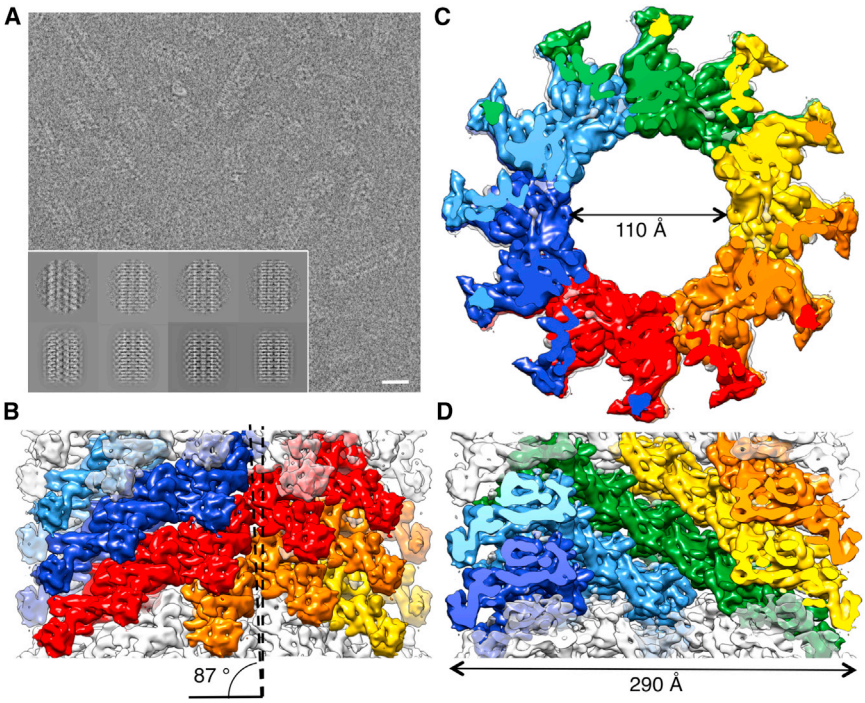

Figure 1. Six-Angstrom Cryo-EM Reconstruction of the Contracted VipA/B Tubule

(A) Inverted micrograph of VipA/B tubules (~−2 μm defocus) taken under low-dose cryo conditions. Scale bar, 30 nm. Class averages containing ~30 aligned images of the final data set obtained by multivariate statistical analysis (inset, upper row) and corresponding reprojections of the final 3D reconstruction in the Euler angle directions assigned to class averages (inset, lower row).

(B–D) 3D reconstruction of VipA/B tubules at 6.0 Å resolution shown as side view (B), top view (C), and cut-open view (D). The six protofilaments are colored separately. Please see also Figure S1 for the resolution determination and Movie S1.

RESULTS

Six-Angstrom Cryo-EM Reconstruction of VipA/B Tubules Shows a Right-Handed Six-Start Helix

We used cryo-EM and single-particle image analysis to determine the structure of the contracted VipA/B tubule at a resolution of 6 Å (Figure 1; Figures S1A and S1B; Movie S1). The tubule is formed by six protofilaments arranged as a right-handed six-start helix with a helical rise of 22.2 Å and a helical turn of 29.44° (Figure S1C). In analogy to early T4 tail sheath characterization (Amos and Klug, 1975), the symmetry can also be described by an assembly of stacked hexameric rings that are rotated by 29.44° from one ring to the other. The layer height of a hexameric T6SS disc measures 44.4 Å and the tubules have an outer diameter of 290 Å, comprising a central channel of 110 Å in diameter. The subunits of one ring are positioned almost exactly in between the subunits of the subjacent ring, resulting in the previously described 12-merous cogwheel-like appearance of short tubules when viewed from the top (Bönemann et al., 2009). The cogs create 12 left-handed ridges with a pitch angle of 87° on the outside of the assembly. In contrast, the T4 phage tail and the published VipA/B tomogram (Basler et al., 2012) display right-handed surface ridges. Our findings also disagree with publications on T6SS tubules that base structural similarity between both systems on the appearance of the surface ridges (Basler et al., 2012; Lossi et al., 2013). Interestingly, our results agree with the description of T6SS like polysheath structures isolated from *Alcaligenes eutrophus* (Walther-Mauruschat and Mayer, 1978), showing left-handed ridges with a pitch angle of 86°. Altogether, the handedness of the tubules, the helical parameters, and the surface dimensions of our VipA/B structure resemble those of contracted T4 phage tails (Table S1). However, a bigger helical rise and smaller helical turn in the VipA/B protofilament indicate that T4 phage tails contract to a greater extent than T6SS tubules. In particular, the rotation angle of 32.9° between the hexameric ring of contracted T4 phage tails results in right-handed surface ridges, whereas the smaller rotation angle of 29.44° results in left-handed surface ridges on VipA/B tubules.

VipA Termini Are Surface Accessible, while the VipB C Terminus Faces the Central Channel

At 6 Å resolution, we are able to clearly identify secondary structure elements, but in order to trace the Cα chains of VipA and VipB, a correct segmentation of the electron microscopy (EM) map is necessary. Without prior knowledge about domain topology or structures of the individual proteins, a segmentation of the helical EM map is impossible (Lander et al., 2012). We thus proceeded to localize VipA and VipB segments in the contracted tubules using a range of hybrid methods. Since tubules are formed from equimolar amounts of VipA and VipB (Bönemann et al., 2009), we can assume that each asymmetric unit is composed of a VipA/VipB heterodimer. Mutational studies suggest that VipA/B interaction is essential for T6S function, involving residues 100–122 in VipA and residues 63–163 in VipB (Aubert et al., 2010; Bröms et al., 2009, 2013) at least. However, neither the crystal structures of VipA or VipB nor of any homologs are known. Limited proteolysis experiments revealed that apart from the C terminus of VipB, all termini are prone to proteolytic digestion by trypsin for up to 63 amino acids (aa) from the protein ends (Figure S2A). Light-scattering experiments and negative-stain EM of early products of proteolytic fragmentation show that, in particular, dismantling of VipA leads to tubule breakdown and aggregation of the proteins (Figures S2B and S2C). The C terminus of VipB and flexible loops within the proteins are protected from proteolytic digestion. Gold labeling of an N-terminal His_6 tag fusion of VipA marks density on the wheel rim of the cogwheel in top views (Figure S2D) but cannot be seen in side views of intact tubules, presumably because the tag is only

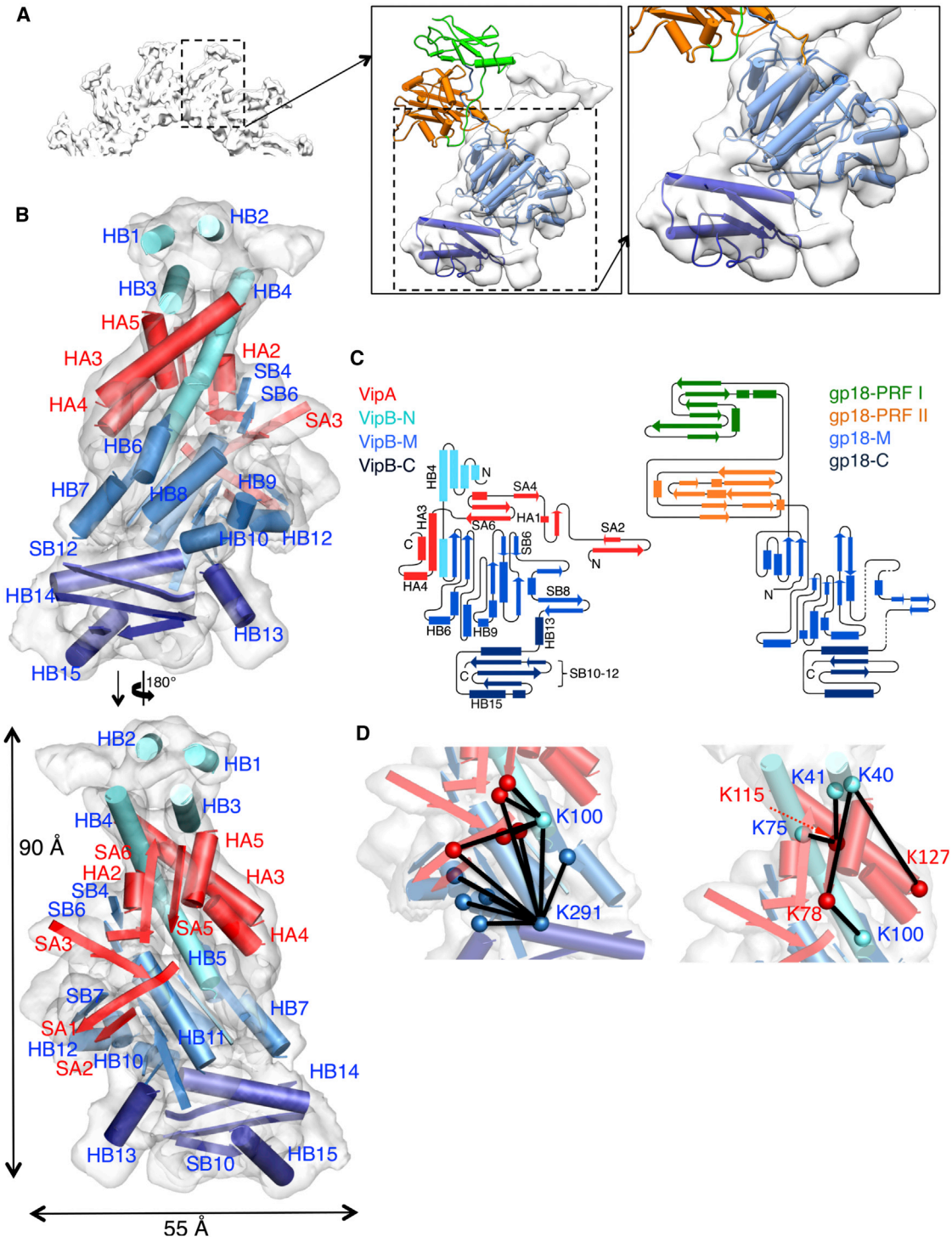

Figure 2. Fit of Secondary Structure Elements and Crosslinking-MS Analysis of VipA/B Protomers

(A) Overlay between gp18 (PDB ID 3J2N) and VipA/B protomer (transparent white) as seen from the top.

(B) Gp18 is color-coded as follows: green, protease resistant fragment (PRF) I; orange, PRF II; blue, middle segment; dark blue, C-terminal segment. Fit of secondary structure elements of VipA (red) and VipB (blue) into VipA/B protomer (transparent white) as seen from the top of the tubule (top) and from the membrane-facing side (bottom). VipB is color-coded as follows: cyan, VipB N-terminal segment; blue, VipB middle segment; dark blue, VipB C-terminal segment. Helices are numbered according to the prediction of PredictProtein (Rost et al., 2004). Structural elements of VipA are labeled xA# and elements of VipB are labeled xB#.

(legend continued on next page)

accessible at tubule ends. Antibodies that bind to a C-terminal hemagglutinin tag fusion of VipA are located on the outside of the tubules in top views of negatively stained complexes (Figure S2E). Furthermore, a yellow fluorescent protein (YFP) moiety fused to the C terminus of VipB is detected in the central channel of the tubules (Figure S2F) (Kapitein et al., 2013). Hence, we established that both termini of VipA are residing on the outside of the contracted tubule, while the C terminus of VipB is oriented toward the central channel.

Fit of Secondary Structure Elements Reveals Unique Domains in VipA and VipB and a Similar Architecture of VipB Core Region and gp18

In order to segment the VipA/B EM map, we made use of our localization of protein termini, secondary structure predictions, homology between VipB and proteins of the gp18 *Myoviridae* bacteriophage family of tail sheath proteins (Aksyuk et al., 2011), and known interactions between VipA and VipB.

Bioinformatic analysis of the C-terminal region of VipB ortholog HsiC1 (282–488) anticipates structural similarity with the C-terminal region of proteins of the gp18 family (Leiman and Shneider, 2012; Lossi et al., 2013) (Protein Data Bank [PDB] ID 3HXL: aa 262–437, 3LML, 3J2N; Figure S3A). Indeed, an overlay between this C-terminal fragment of gp18 and the channel facing densities in our right-handed EM map discloses a very good fit for the large β sheet density and two distinct α-helical densities (Figure S3B). A structure prediction (Söding, 2005) of this region based on remote sequence homology to gp18 fits the channel-facing densities of our EM map equally well (Figure S3C). We therefore conclude that the C-terminal segment of VipB constitutes the inner wall of the tubules, analogous to gp18 in the T4 phage tail sheath (Aksyuk et al., 2009).

Despite the lack of any detectable sequence homology, we identify a similar overall architecture between the gp18 structures devoid of the protease resistant insertions (PRF) and residues 170 to 492 of VipB (Figures 2A–2C; Movie S2). Thus, starting at the C terminus of VipB, we manually traced back the peptide chain along the scaffold of the bacteriophage crystal structures and fitted secondary structure elements of the VipB-M (middle) and VipB-C (C-terminal) segments comprising β sheet SB12 to SB1 (Figures 2B and 2C; Figure S4). The structural similarity between gp18 and VipB diminishes with the transition from gp18 core regions to PRF domains, which corresponds to the C-terminal segment of helix 5 in VipB (Movie S3). Yet, at the resolution of our map, it is possible to fit the remaining five helices of VipB with high confidence. Ab initio structure modeling using Quark (Xu and Zhang, 2012) returned a four-α helix bundle for helices HB1–4 that can easily and only be placed into the α-helical EM density of the cogs (Figure S3D). This location of the VipB N terminus also agrees with our limited proteolysis data. The distance between the four-helix bundle and the VipB core region is bridged by helix HB5, which fits into a well-defined α-helical density in our map. Thus, VipB is divided into a core region, homologous to gp18, and an N-terminal region that carries the recognition motif for ClpV on HB2 (residues 13–31 of VipB) (Pietrosiuk et al., 2011) presenting it on the outside of the contracted T6SS tubules.

The remaining density in our EM map can be attributed to VipA. VipA wraps around helix HB5 of VipB, seemingly reinforcing the bridge between VipB core regions and the N terminus. While gp18 domains are clearly separated by loop regions, VipB forms a compact structure in interaction with VipA. Secondary structure predictions show that VipA is divided into a β sheet-rich N-terminal part and an α-helical C-terminal part. Positioning of VipA into the remaining EM density was guided by the 25-residue-long α helix HA3, which only fits one location of this density (Figure 2B; Figure S4). In our fit, the α-helical part of VipA contacts helix HB4 and HB5 of VipB and the β sheet-rich portion comes to lay on top of helix HB11 and β sheets SB4–SB7 (Figure 2B). Interestingly, our fit of VipA not only agrees with previously published interaction data (Bröms et al., 2009, 2013; Zhang et al., 2013) but also would allow for a fusion between VipA and VipB as seen in some proteobacteria such as *Burkholderia glumae* or *Hylemonella gracilis*. In all fusion proteins, the VipA C terminus is linked directly or by a short peptide sequence to the N terminus of VipB.

In order to independently verify our segmentation and fit, we analyzed VipA/B protomers by chemical crosslinking of lysines (VipA contains 14, VipB 29) combined with mass spectrometry (MS), comprising full-length or truncated versions of VipB, which lack the C-terminal region (Table S2). VipBΔC^{210} and VipBΔC^{367} are soluble and dimerize with VipA but are unable to form tubules, and crosslinks observed in these variants only reveal intraprotomer interactions. In the three experiments cross- and monolinks for 13 out of the 14 lysines of VipA and 26 out of the 29 lysines of VipB were obtained. Altogether, we obtained 83 crosslink pairs, 65 of which were distinct. Out of these crosslinks, 34 were VipA-VipA pairs, 19 were VipA-VipB pairs, and 12 were VipB-VipB pairs. In our fit, all distances but one between Cα-atoms of the crosslinked lysines fell below 31 Å. In fact, 36 crosslinking pairs show Cα-distances of less than 21 Å, corresponding to the linker (7.7 Å) plus two times the length of a lysine side chain (6.5 Å), and 28 crosslinking pairs show Cα-distances between 21 and 31 Å. Given that our fit is based on predicted secondary structure elements that have been built de novo and that lysines in loop regions cannot be placed precisely into the EM map, the crosslinking analysis supports our fit at large. In particular, the central position of helices HB11 (K291) and HB5 (K100) was verified by numerous crosslinks to neighboring lysines in the N-terminal region of VipA and the C-terminal region of VipB (Figure 2D). Helix 3 of VipA (residues 103–127) forms

(C) Topology diagram of VipA and VipB as fitted into the EM density (left) and of gp18 as derived from PDB ID 3J2N (right). VipA/B is color-coded as in (B), and gp18 is color coded as in (A).

(D) Observed crosslinks in deletion mutants VipA/VipBΔC210, VipA/VipBΔC367, or wild-type VipA/B involving K291 and K100 of VipB (left) and interprotein crosslinks between lysines of VipA and the N-terminal segment of VipB (right). Fitted secondary structure elements of the VipA/B protomer as depicted in (B) are shown. The Cα atoms of lysines are depicted as spheres, and crosslinks are indicated by black lines.

See also Figures S2–S4 and Movies S2 and S3.

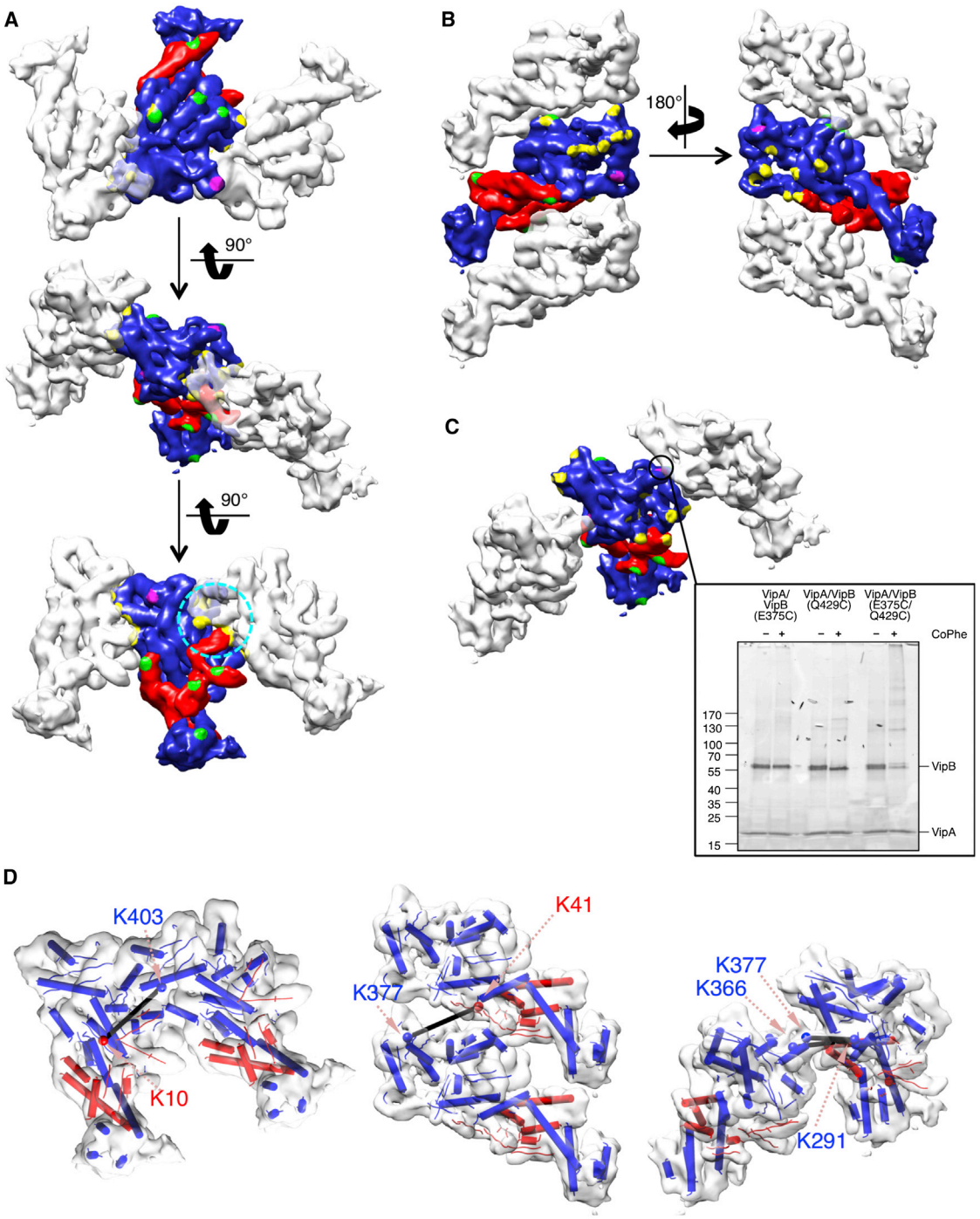

Figure 3. Interprotomer Contacts in Contracted VipA/B Tubules

(A–C) Neighboring protomers as based on segmentation of the filtered VipA/B map are depicted for intraprotofilament contacts (A) and interprotofilament contacts (B and C).

(A) Segment of three consecutive protomers of a protofilament indicating intraprotofilament contacts shown as top view, inside-out, and bottom view. One protomer is segmented into VipA (red) and VipB (blue) densities. The area corresponding to the proposed intraprotofilament contact area (Aksyuk et al., 2009) in T4 is marked by a cyan circle.

(B) Interprotofilament contacts between protomers that lie on top of each other are depicted as side views.

(C) Interprotofilament contacts between protomers of adjacent hexameric rings are shown as seen from inside the tubules. Interprotofilament contacts in between VipA/VipB-E375C/Q429C under oxidizing conditions. Oxidized VipB single-cysteine variants and reducing conditions are given as control (inset). Contact

(legend continued on next page)

three crosslinks with helices HB3 or HB4 of VipB (Figure 2D). The N-terminal segment between HB3 and HB8 of VipB was proposed to mediate VipA interaction (Aubert et al., 2010). Our fit and crosslinking data confirm that HB3-SB1 of VipB directly interact with VipA.

VipB-VipB Interactions Stabilize Protofilaments, and VipA Interacts Only with VipB

Provided with a secondary structure model of the heterodimer, we examined the contact points between individual protomers in order to identify residues important for tubule stability (Figures 3A–3C). Visual inspection of the contact areas on the map surface reveals that most contacts are formed between neighboring protomers in a protofilament (Figure 3, yellow marks), thereby stabilizing the structure. A loop region and β hairpin preceding and succeeding the α helix homologous to helix HB11 in VipB were suggested to form crucial contacts during contraction of the viral tail sheath (Aksyuk et al., 2009). Interestingly, in our VipA/B structural model, the VipA N terminus occupies the corresponding position in between protomers of the tubular structure (Figure 3A, cyan circle), indicating that VipA might sense or participate in tubule contraction. In contrast to intraprotofilament contacts, which are predominantly mediated by VipB/VipB interactions, interprotofilament contacts between protomers that come to lie on top of each other are exclusively mediated by VipA/VipB interactions (Figure 3B). Based on our structural model of the VipA/B protomer, these interprotofilament contacts involve the β sheet-rich N terminus of VipA, HA3, a loop region between helices HA3 and HA4 of VipA, and loop regions before helices 7, 8, and 9 of VipB (Figure 3, green marks; Figure S4). Another contact between neighboring protofilaments is made between protomers of consecutive hexameric rings (Figure 3C). This VipB/VipB contact involves helix HB15 and the loop preceding helix HB13 (Figure 3, magenta marks). We validated this interprotomer contact by in vitro crosslinking using engineered cysteines at E375 in the loop before HB13 and Q429 in HB15 of VipB (Figure 3C).

Furthermore, our chemical crosslinking and MS analysis of the full-length VipA/B tubules yielded four crosslink pairs whose Cα distances agree better with interprotomer than with intraprotomer crosslinks (Figure 3D).

VipB N Terminus Is Embedded in the Tubule Wall in a Model of Elongated T6S Tubule

The structural details of tubule formation by VipA/B and the mechanism of contraction are poorly understood. Neither the structure nor the helical parameters of the extended T6SS tubules have been solved. Based on in situ measurements in cryotomograms, it was suggested that the contracted T6SS tubules collapse to 55.8% of the length of the extended tubules and expand to 126% of their width (Basler et al., 2012).

Comparison of the helical structure of the contracted T4 phage tail with the VipA/B tubule suggests that the T4 sheath contracts further than VipA/B tubules (Figure 4A). Indeed, contracted T4 sheaths collapse to 45% of the extended sheath and expand to 138% of their width (Leiman et al., 2010). In order to investigate whether our EM map represents the final state of contraction of VipA/B tubules, we compared the protofilament arrangement in our map with that of T4 phage tails (Figure S5A). Consecutive subunits of the T4 sheath protofilament perform an almost 30° in-plane rotation between the extended and contracted state, resulting in a stronger curvature described by their C-terminal domains. This movement is accompanied by a slight rotation around the long axis of the protomer, causing a shallower rise between protomers in the contracted filament. The in-plane rotation between neighboring protomers in the VipA/B protofilament and in the contracted T4 sheath is almost identical, showing that our VipA/B assembly reflects the contracted state of the T6SS.

We were interested to understand why T4 sheaths can contract further than VipA/B tubules. Therefore, we fitted the VipA/B protomers into the contracted T4 tail sheath by overlaying the structurally conserved segments of both protomers. While VipA/B subunits within one protofilament do not show significant clashes when built upon symmetry parameters of contracted T4 sheaths, protomers that come to lie on top of each other clash considerably (Figure S5B). The clashes mainly involve densities attributed to VipA, indicating that this VipB-stabilizing protein restricts further contraction of VipA/B tubules by preventing tighter packing of neighboring protofilaments.

In order to test whether elongated T6SS tubules can be built upon analogy to the T4 phage tail, we fitted similar regions of VipA/B protomers and gp18 crystal structures (Fokine et al., 2013) into the low-resolution cryo-EM structure of the extended T4 phage tail (Figure 4A). Although we cannot rule out changes in the tertiary structure of the protomer during contraction, this approach is based on the current model of T4 phage tail contraction, which is described as rigid-body movement of the individual subunits (Leiman and Shneider, 2012). The protomers are accommodated in the modeled structure without major clashes, despite the varying overall architectures of VipB and gp18. The different orientations of the unique domains lead to a strikingly different appearance of the two elongated tubular structures. While the protease-resistant fragments of gp18 protrude from the phage tail, the unique N-terminal four-helix bundle of VipB is embedded in the tubule wall, giving the extended T6SS tubule a smooth outside surface (Figures 4A and 4B). Recently, we identified an α helix in the N-terminal region of VipB that interacts with the N-terminal domains of ClpV (Pietrosiuk et al., 2011). Our structural model of the VipA/B protomer predicts that the ClpV recognition motif is presented in the cogs of the tubules in the contracted state (Figure 4A, green asterisk). In order to

areas for protomer-protomer contacts are highlighted as follows: yellow, intraprotofilament contacts as seen in (A); green, interprotofilament contacts as seen in (B); magenta, interprotofilament contacts as seen in (C).

(D) Intraprotofilament (left) and interprotofilament (middle and right) crosslinks as derived from the crosslinking-MS analysis of wild-type VipA/B tubules. Two protomers with fitted secondary structure elements of VipA (red) and VipB (blue) are shown in the same orientations as seen in (A–C). The Cα atoms of crosslinked residues are depicted as spheres, and crosslinks are indicated by black lines.

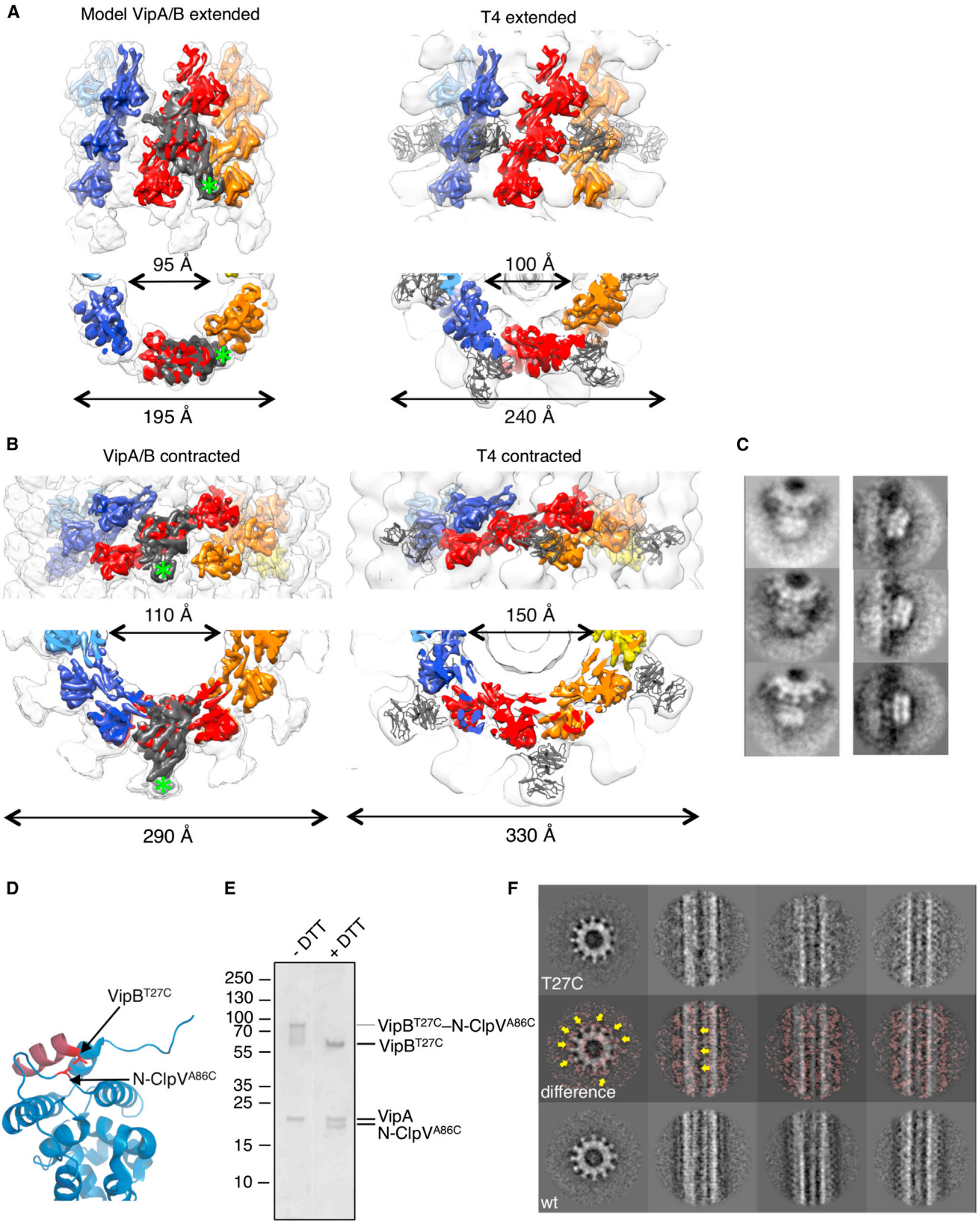

(legend on next page)

locate the ClpV binding site in VipA/B tubules, we analyzed them in the presence of ClpV and ATPγS (Figure 4C). Class averages of negatively stained complexes show that ClpV indeed binds to the cogs of the cogwheels. Furthermore, we specifically crosslinked introduced cysteines VipB^{T27C} and ClpV^{A86C} in the binding motifs of both proteins and showed that the ClpV N termini preferentially bind to one side of the VipA/B cogs (Figures 4D–4F). While it is presented in the cogs of the contracted tubules, the ClpV recognition motif is buried between neighboring protofilaments in the elongated model of the VipA/B tubules (Figure 4B, green asterisk) and is presumably shielded from the disaggregase.

DISCUSSION

The contractile VipA/B tubule plays the central role in type VI effector secretion. In the current model, the contraction of the tubule provides enough energy to pierce bacterial membranes and inject effector molecules into neighboring target cells (Basler et al., 2013). Despite speculation about functional similarities between T6SS tubules and bacteriophage tail sheaths (Basler et al., 2012; Leiman et al., 2009), the structures of VipA, VipB, and its helical assembly had been unknown. With regard to tubule contraction, it remains to be proven to what extent functional similarities between the two systems hold true. On the one hand, the lack of high-resolution structures of sheath assemblies prevents elucidation of the exact mechanism of T4 tail sheath contraction, and on the other hand obvious differences between both systems, such as varying length of the tubular structures, might reflect mechanistic variations.

First proof of structural similarity between T6SS tubules and T4 phage tails comes from the overall architecture of the contracted tubules (see helical symmetry parameters in Table S1) (Leiman et al., 2004). VipA/B tubules and T4 phage tails adopt the same handedness in their six-start helical assembly (Aksyuk et al., 2009), even though the surface ridges show opposite handedness due to differences in the extent of contraction. Furthermore, only the core regions of T4 tail sheath protein gp18 and VipB, which mediate intraprotofilament contacts and thus define the helical array, show structural conservation. Although weak, the greatest homology between T4 phage tail proteins and VipB is found in VipB-C. This region was shown to be crucial for tubule formation in *Pseudomonas aeruginosa* (Lossi et al., 2013), and we can confirm this observation for *vc*VipA/VipBΔC^{367} protomers (data not shown). We conclude that these structurally conserved core regions of gp18 and VipB are responsible for the common function of maintaining the sheath integrity as it was proposed for the T4 phage (Leiman et al., 2010).

Examination of protofilament contacts during contraction substantiates this statement. For T4 phages, it was observed that the number of contacts between neighboring subunits within a protofilament remain more or less constant, while contacts between neighboring protofilaments increase during contraction (Aksyuk et al., 2009; Leiman et al., 2010). Based on the structural conservation between gp18 and VipB, we could model the extended state of VipA/B tubules using the low-resolution cryo-EM structures of the T4 tail sheath. Comparison of the protofilament arrangement in the elongated model and contracted density map shows that the C-terminal domains maintain close contact throughout contraction. However, contraction also triggers an in-plane rotation between consecutive protomers in the protofilament, indicating that the interface between neighboring VipB-C domains is altered upon contraction. Hence, we assume that rather than the advance of peripheral contacts, a structural change in the protomer perpetuates throughout each protofilament and drives tubule contraction. The structurally conserved C-terminal segments of T4 phage tail proteins and VipB could initiate this structural switch, since they are found at the core of the observed changes while maintaining protofilament contacts.

In contrast to VipB, VipA shows no structural relationship to viral tail sheath proteins, which raises the question about its purpose. Since stable expression of VipB in *V. cholerae* requires the presence of VipA and the VipA/B heterodimer is restored immediately after ClpV-mediated tubule disassembly (Bönemann et al., 2009), VipA might function as a chaperone to keep VipB in solution. Indeed, our structure suggests that VipA stabilizes VipB by helping to bridge the distance between the VipB core region and the N-terminal domain, thereby creating a compact heterodimeric structure. In contrast to viral tail sheaths, which often contain PRF domains (Aksyuk et al., 2011) in order to be

Figure 4. Comparison between T6SS Tubules and T4 Phage Tail Sheaths

(A) Model of the extended VipA/B tubule based on fit to the extended T4 tail sheath seen as a side view (top left) and cut-away top view (bottom left). Overlay between the hexameric gp18 model (PDB ID 3J2M, gray) and the extended T4 sheath EM map (EMD-1126, transparent white) shown as a side view (top right) and cut-away top view (bottom right). The hexameric gp18 model was fitted into three consecutive rings of the elongated T4 sheath, and low-pass-filtered middle and C-terminal segments (colored) were used to model the elongated VipA/B tubule based on best fit between the homologous segments. Low-pass-filtered protofilament segments are colored separately. One hexameric gp18 model is depicted as gray crystal structure. One VipA/B protomer is rendered at a high threshold to illustrate the overlay and location of helix 2 of VipB (green star).

(B) Comparison of the contracted VipA/B tubule (left) with the contracted T4 tail sheath (EMD-1086; right) seen as a side view (upper row) and cut-away top view (lower row). The color code for EM maps, crystal structures, and low-pass-filtered segments are as in (A). PDB ID 3J2N was used as hexameric gp18 model.

(C) Top view (left) and side view (right) class averages of VipA/B tubules bound to ClpV in the presence of ATPγS.

(D) Location of cysteine residues used for crosslinking between VipB and the N terminus of ClpV shown on the basis of the crystal structure PDB ID 3ZRJ. The ClpV N terminus is colored in blue, and the VipB peptide is colored in red.

(E) Reduced and oxidized (±DTT) VipA/B/ClpV-N assemblies were analyzed by nonreducing SDS-PAGE. Intramolecular disulfide crosslinks were visualized by band upshifts in SDS-PAGE.

(F) Class averages of negatively stained VipA/B tubules crosslinked to ClpV-N (upper row). The images were binarized and overlaid with images of class averages of negatively stained wild-type VipA/B tubules (middle row). Additional density is colored in red and indicated by yellow arrows. Class averages of negatively stained wild-type VipA/B tubules (lower row).

See also Figure S5.

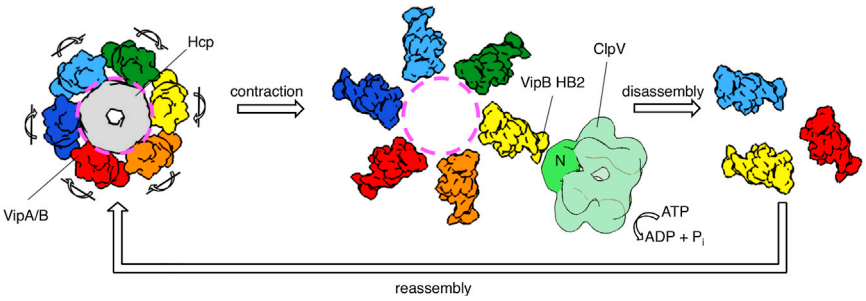

Figure 5. Model for T6SS Tubule Recycling
The elongated VipA/B tubule (left) encloses the needle complex formed by Hcp (gray). Upon contraction, the VipA/B protomers (green, yellow, orange, red, blue, and light blue) rotate outward, thereby presenting the VipB N terminus to ClpV (light green). The contracted VipA/B tubule is disassembled by ClpV, and free VipA and VipB can reassemble to form newly loaded T6S complexes.

protected against extracellular proteases, VipB presents a recognition motif for recycling by ClpV in the N-terminal domain on the outside of the contracted T6SS tubule. This recognition motif is attached to the core region of VipB by a long α helix (HB5), instead of flexible loop regions as seen for viral PRF domains. VipA clamps around helix HB4 and HB5 of VipB and fastens the steric arrangement. It is plausible that the compact architecture of the heterodimer enhances efficiency of disaggregation, as tractive force applied at the N-terminal domain will directly be transferred into the core of VipB to destabilize protofilament interactions. In particular, pulling on HB5 would impact on a central β sheet (SB1) of the VipB core. Thus, partial unfolding of and pulling on VipB might be sufficient to disassemble T6SS tubules and set free VipA/B heterodimers, explaining their quick re-emergence after ClpV disassembly. Intriguingly, ClpV only seems to target VipB while hybrid complexes of the ClpV N-terminal domain coupled to ClpA/P leave VipA untouched (Pietrosiuk et al., 2011). The distinctive N-terminal domain of VipB therefore would act as a recycling domain for T6SS tubules, providing the ClpV recognition motif, an interaction surface for VipA, and a structural link to the VipB core. VipA, on the other hand, would stabilize and protect the structurally conserved VipB core region.

One drawback of VipA-mediated VipB stabilization is the increased size of the protomer compared to gp18, which results in less compact packing of the contracted protofilaments. Consequently, over a given number of protomers, T6SS tubules contract less than T4 phage tails, possibly causing a reduction in injection power. However, since extended VipA/B tubules are about seven times longer than extended T4 phage tails (Basler et al., 2012), the bacterial system's shortcomings in contraction can be compensated for by its length.

Finally, our model of the extended VipA/B tubule reveals why ClpV only targets contracted tubules for disaggregation. When built upon the same helical array as the extended T4 tail sheath, the unique protomer architecture of VipA/B causes the N-terminal domain of VipB to be buried in the tubule wall instead of projecting away from the tubule as seen for viral PRF domains. The ClpV recognition motif is thereby inaccessible for the disaggregase, and extended tubules are protected from premature disassembly (Figure 5). In the contracted state, the VipB N termini are located in the cogs of the tubule and are easily accessible to ClpV. Thus, contraction-state-dependent positioning of the unique N-terminal recycling domain of VipB enables disaggregation of the tubules only after contraction and ensures reusage of VipA/B.

EXPERIMENTAL PROCEDURES

For more detailed descriptions, please see Supplemental Experimental Procedures.

Protein Purification, Tryptic Digestion, and Cysteine Crosslinking

VipA/VipB wild-type, tagged, and VipB truncation mutant complexes were purified as described previously (Bönemann et al., 2009; Pietrosiuk et al., 2011). For VipA/VipB-YFP, gel filtration was substituted by glycerol-gradient ultracentrifugation. The cysteine mutants were purified without reducing agents present. Additionally, VipA/VipB mutants E375C, Q429C, and E375C/Q429C were reduced with tris(2-carboxyethyl)phosphine and reoxidized with copper phenanthroline. Tryptic digest was performed in purification buffer, and fragments were identified by mass spectrometry and N-terminal sequencing (Toplab).

Chemical Crosslinking and Mass Spectrometry

Wild-type and VipB truncation mutant complexes were crosslinked with disulfosuccinimidyl-glutarate (Creative Molecules) and analyzed as described in Herzog et al. (2012).

Electron Microscopy and 3D Reconstruction

Ni-NTA-Nanogold (Nanoprobes) labeling was performed as specified by the manufacturer. Negative staining of the tubules was either done with 2% (w/v) uranyl acetate or Nano-W (Nanoprobes). Cryo-EM images were taken under low-dose conditions at 200 keV on a Titan Krios transmission electron microscope equipped with a TEMCAM-F416 CMOS camera. A total of 12,271 micrographs were collected by semiautomated data collection ranging between −1,000 and −4,500 nm in defocus. The final 3D reconstruction comprised 16,394 particle images and has a resolution of 5.8 Å (Fourier shell correlation = 0.5).

Map Segmentation and Atomic Structure Fitting

Segmentation and manual fitting of secondary structure elements were performed using UCSF Chimera (Pettersen et al., 2004) and Segger (Pintilie et al., 2010) with viral tail sheath structures 3J2N, 3LML, and 3HXL as templates.

Map Visualization

All cryo-EM densities and structures were visualized in UCSF Chimera (Pettersen et al., 2004) except for Figures 2B and 2D, which were created in PyMOL (The PyMOL Molecular Graphics System, MacPymol Schrödinger).

ACCESSION NUMBERS

The 3D reconstruction and a segmented VipA/B protomer have been deposited to the Electron Microscopy Data Bank (EMDB) under accession codes EMD-2524 and EMD-2525, respectively.

SUPPLEMENTAL INFORMATION

Supplemental Information includes Supplemental Experimental Procedures, five figures, three tables, and three movies and can be found with this article online at http://dx.doi.org/10.1016/j.celrep.2014.05.034.

AUTHOR CONTRIBUTIONS

S.K., P.W., N.K., and A.M. designed and performed all the biochemical experiments. The EM and three-dimensional image analysis was performed by S.K. and P.W. T.Z. and F.H. performed mass spectrometric analyses. S.K., P.W., N.K., and A.M. contributed to data interpretation and manuscript preparation. S.K. and P.W. wrote the manuscript.

ACKNOWLEDGMENTS

We thank Elena Orlova and Naoko Mizuno for helpful discussions and Patrick Cramer for critical reading of the manuscript. We also wish to thank Jana Albrecht and Tobias Hassler for technical assistance, Andreas Hauser for computing support, and Otto Berninghausen and Charlotte Ungewickell for data collection on the Titan Krios. Nicole Kapitein was supported by the Hartmut Hoffmann-Berling International Graduate School of Molecular and Cellular Biology. Work in the lab of F.H. is supported by the Bavarian Research Center for Molecular Biosystems, the Graduate School 1721 (German Research Foundation), and by an LMU*excellent* Junior grant. This work was supported by grants from the German Research Council (DFG) to A.M. (MO970/3) and P.W. (WE 4628/1, GRK1721).

Received: January 9, 2014
Revised: April 16, 2014
Accepted: May 16, 2014
Published: June 19, 2014

REFERENCES

Aksyuk, A.A., Leiman, P.G., Kurochkina, L.P., Shneider, M.M., Kostyuchenko, V.A., Mesyanzhinov, V.V., and Rossmann, M.G. (2009). The tail sheath structure of bacteriophage T4: a molecular machine for infecting bacteria. EMBO J. *28*, 821–829.

Aksyuk, A.A., Kurochkina, L.P., Fokine, A., Forouhar, F., Mesyanzhinov, V.V., Tong, L., and Rossmann, M.G. (2011). Structural conservation of the myoviridae phage tail sheath protein fold. Structure *19*, 1885–1894.

Amos, L.A., and Klug, A. (1975). Three-dimensional image reconstructions of the contractile tail of T4 bacteriophage. J. Mol. Biol. *99*, 51–64.

Aubert, D., MacDonald, D.K., and Valvano, M.A. (2010). BcsKC is an essential protein for the type VI secretion system activity in Burkholderia cenocepacia that forms an outer membrane complex with BcsLB. J. Biol. Chem. *285*, 35988–35998.

Basler, M., Pilhofer, M., Henderson, G.P., Jensen, G.J., and Mekalanos, J.J. (2012). Type VI secretion requires a dynamic contractile phage tail-like structure. Nature *483*, 182–186.

Basler, M., Ho, B.T., and Mekalanos, J.J. (2013). Tit-for-tat: type VI secretion system counterattack during bacterial cell-cell interactions. Cell *152*, 884–894.

Bönemann, G., Pietrosiuk, A., Diemand, A., Zentgraf, H., and Mogk, A. (2009). Remodelling of VipA/VipB tubules by ClpV-mediated threading is crucial for type VI protein secretion. EMBO J. *28*, 315–325.

Bröms, J.E., Lavander, M., and Sjöstedt, A. (2009). A conserved alpha-helix essential for a type VI secretion-like system of Francisella tularensis. J. Bacteriol. *191*, 2431–2446.

Bröms, J.E., Ishikawa, T., Wai, S.N., and Sjöstedt, A. (2013). A functional VipA-VipB interaction is required for the type VI secretion system activity of Vibrio cholerae O1 strain A1552. BMC Microbiol. *13*, 96.

Cascales, E., and Cambillau, C. (2012). Structural biology of type VI secretion systems. Philos. Trans. R. Soc. Lond. B Biol. Sci. *367*, 1102–1111.

Coulthurst, S.J. (2013). The Type VI secretion system - a widespread and versatile cell targeting system. Res. Microbiol. *164*, 640–654.

Fokine, A., Zhang, Z., Kanamaru, S., Bowman, V.D., Aksyuk, A.A., Arisaka, F., Rao, V.B., and Rossmann, M.G. (2013). The molecular architecture of the bacteriophage T4 neck. J. Mol. Biol. *425*, 1731–1744.

Hayes, C.S., Aoki, S.K., and Low, D.A. (2010). Bacterial contact-dependent delivery systems. Annu. Rev. Genet. *44*, 71–90.

Herzog, F., Kahraman, A., Boehringer, D., Mak, R., Bracher, A., Walzthoeni, T., Leitner, A., Beck, M., Hartl, F.U., Ban, N., et al. (2012). Structural probing of a protein phosphatase 2A network by chemical cross-linking and mass spectrometry. Science *337*, 1348–1352.

Kapitein, N., Bönemann, G., Pietrosiuk, A., Seyffer, F., Hausser, I., Locker, J.K., and Mogk, A. (2013). ClpV recycles VipA/VipB tubules and prevents non-productive tubule formation to ensure efficient type VI protein secretion. Mol. Microbiol. *87*, 1013–1028.

Lander, G.C., Saibil, H.R., and Nogales, E. (2012). Go hybrid: EM, crystallography, and beyond. Curr. Opin. Struct. Biol. *22*, 627–635.

Leiman, P.G., and Shneider, M.M. (2012). Contractile tail machines of bacteriophages. Adv. Exp. Med. Biol. *726*, 93–114.

Leiman, P.G., Chipman, P.R., Kostyuchenko, V.A., Mesyanzhinov, V.V., and Rossmann, M.G. (2004). Three-dimensional rearrangement of proteins in the tail of bacteriophage T4 on infection of its host. Cell *118*, 419–429.

Leiman, P.G., Basler, M., Ramagopal, U.A., Bonanno, J.B., Sauder, J.M., Pukatzki, S., Burley, S.K., Almo, S.C., and Mekalanos, J.J. (2009). Type VI secretion apparatus and phage tail-associated protein complexes share a common evolutionary origin. Proc. Natl. Acad. Sci. USA *106*, 4154–4159.

Leiman, P.G., Arisaka, F., van Raaij, M.J., Kostyuchenko, V.A., Aksyuk, A.A., Kanamaru, S., and Rossmann, M.G. (2010). Morphogenesis of the T4 tail and tail fibers. Virol. J. *7*, 355.

Lossi, N.S., Dajani, R., Freemont, P., and Filloux, A. (2011). Structure-function analysis of HsiF, a gp25-like component of the type VI secretion system, in Pseudomonas aeruginosa. Microbiology *157*, 3292–3305.

Lossi, N.S., Manoli, E., Förster, A., Dajani, R., Pape, T., Freemont, P., and Filloux, A. (2013). The HsiB1C1 (TssB-TssC) complex of the Pseudomonas aeruginosa type VI secretion system forms a bacteriophage tail sheathlike structure. J. Biol. Chem. *288*, 7536–7548.

Mougous, J.D., Cuff, M.E., Raunser, S., Shen, A., Zhou, M., Gifford, C.A., Goodman, A.L., Joachimiak, G., Ordoñez, C.L., Lory, S., et al. (2006). A virulence locus of Pseudomonas aeruginosa encodes a protein secretion apparatus. Science *312*, 1526–1530.

Pettersen, E.F., Goddard, T.D., Huang, C.C., Couch, G.S., Greenblatt, D.M., Meng, E.C., and Ferrin, T.E. (2004). UCSF Chimera—a visualization system for exploratory research and analysis. J. Comput. Chem. *25*, 1605–1612.

Pietrosiuk, A., Lenherr, E.D., Falk, S., Bönemann, G., Kopp, J., Zentgraf, H., Sinning, I., and Mogk, A. (2011). Molecular basis for the unique role of the AAA+ chaperone ClpV in type VI protein secretion. J. Biol. Chem. *286*, 30010–30021.

Pintilie, G.D., Zhang, J., Goddard, T.D., Chiu, W., and Gossard, D.C. (2010). Quantitative analysis of cryo-EM density map segmentation by watershed and scale-space filtering, and fitting of structures by alignment to regions. J. Struct. Biol. *170*, 427–438.

Pukatzki, S., Ma, A.T., Revel, A.T., Sturtevant, D., and Mekalanos, J.J. (2007). Type VI secretion system translocates a phage tail spike-like protein into target cells where it cross-links actin. Proc. Natl. Acad. Sci. USA *104*, 15508–15513.

Records, A.R. (2011). The type VI secretion system: a multipurpose delivery system with a phage-like machinery. Mol. Plant Microbe Interact. *24*, 751–757.

Rost, B., Yachdav, G., and Liu, J. (2004). The PredictProtein server. Nucleic Acids Res. *32* (Web Server issue), W321–W326.

Shneider, M.M., Buth, S.A., Ho, B.T., Basler, M., Mekalanos, J.J., and Leiman, P.G. (2013). PAAR-repeat proteins sharpen and diversify the type VI secretion system spike. Nature *500*, 350–353.

Silverman, J.M., Agnello, D.M., Zheng, H., Andrews, B.T., Li, M., Catalano, C.E., Gonen, T., and Mougous, J.D. (2013). Haemolysin coregulated protein

is an exported receptor and chaperone of type VI secretion substrates. Mol. Cell *51*, 584–593.

Söding, J. (2005). Protein homology detection by HMM-HMM comparison. Bioinformatics *21*, 951–960.

Walther-Mauruschat, A., and Mayer, F. (1978). Isolation and characterization of polysheaths, phage tail-like defective bacteriophages of Alcaligenes eutrophus H 16. J. Gen. Virol. *41*, 239–254.

Xu, D., and Zhang, Y. (2012). Ab initio protein structure assembly using continuous structure fragments and optimized knowledge-based force field. Proteins *80*, 1715–1735.

Zhang, X.Y., Brunet, Y.R., Logger, L., Douzi, B., Cambillau, C., Journet, L., and Cascales, E. (2013). Dissection of the TssB-TssC interface during type VI secretion sheath complex formation. PLoS ONE *8*, e81074.